Journal of Alloys and Compounds 523 (2012) 176–181

Contents lists available at SciVerse ScienceDirect

Journal of Alloys and Compounds

journal homepage: www.elsevier.com/locate/jallcom

Synthesis, magnetic, transport, and thermodynamic investigation of $CeCo(Sb, Sn)_3$

W. Adam Phelan[a], Giang V. Nguyen[a], J.F. DiTusa[b], Julia Y. Chan[a,*]

[a] Department of Chemistry, Louisiana State University, Baton Rouge, LA 70803, United States
[b] Department of Physics and Astronomy, Louisiana State University, Baton Rouge, LA 70803, United States

ARTICLE INFO

Article history:
Received 2 December 2011
Received in revised form 24 January 2012
Accepted 28 January 2012
Available online 9 February 2012

Keywords:
Crystal growth
X-ray diffraction
Intermetallics
Kondo effect
Crystal field

ABSTRACT

$CeCo(Sb, Sn)_3$ has been grown from Sn flux and characterized by single-crystal X-ray diffraction. The crystal structure of $CeCo(Sb, Sn)_3$ adopts the $LaPdSb_3$ structure-type and the structure is comprised of layers $^2_\infty[CoX_2]$ octahedra, where X = Sb and Sb, and nearly square nets of $^2_\infty[X]$ which are separated by Ce atoms. $CeCo(Sb, Sn)_3$ displays a metallic resistivity and the magnetic susceptibility data show paramagnetic behavior down to 2.25 K. Specific heat measurements reveal a phase transition at approximately 2 K, which is most likely magnetic. A Sommerfeld coefficient, $\gamma = 140\ mJ/K^2\ mol\text{-}CeCo(Sb, Sn)_3$, was obtained by fitting the heat capacity data at low temperatures for $CeCo(Sb, Sn)_3$ and is indicative of enhanced charge carrier mass; however, the low temperature resistivity and magnetoresistance data do not support the formation of an enhanced mass state for $CeCo(Sb, Sn)_3$. Thus, the enhanced Sommerfeld coefficient likely results from low lying crystal field levels which give rise to Schottky contributions at low temperatures rather than the formation of heavy quasiparticles. Herein, we report the crystal growth, structure, and physical properties for $CeCo(Sb, Sn)_3$.

1. Introduction

Ternary lanthanide–transition metal–antimonide systems display unusual geometric networks and bonding patterns [1–3]. Additionally, these systems are known to exhibit a wide variety of interesting physical properties [4]. For example, the highly correlated skutterudite $CeFe_4Sb_{12}$ exhibits a thermoelectric efficiency (zT) greater than 1.0 in a high temperature region [5–7]. Another interesting class of Sb-containing phases is the Ce–Ni–Sb ternary intermetallics. α-$CeNiSb_3$ and β-$CeNiSb_3$ both display Kondo lattice behavior around 25 K and order ferromagnetically with $T_c \sim 6$ K [8,9]. These properties are interesting because the occurrence of ferromagnetism in Ce-containing compounds, which display features of Kondo screening at higher temperatures may be indicative of an undercompensated or underscreened Kondo lattice. These conditions have been predicted and experimentally shown to result in the formation of a singular Fermi liquid [10]. Additionally, the ferromagnetic transition temperature of α-$CeNiSb_3$ was found to increase under applied pressures up to 25 kbar, decrease for applied pressure greater than 25 kbar, and a second ferromagnetic ordered phase emerged between pressure between 35 kbar and 55 kbar. The existence quantum critical point (QCP) at $P \sim 60$ kbar was suggested due to the nearly complete suppression of the first magnetic phase and an increase in the T^2 coefficient and ρ_0 observed from fits to electrical resistivity at this pressure [11].

More recently, $CeCoSb_3$, which adopts the $LaPdSb_3$ structure-type and is isostructural to β-$CeNiSb_3$, was prepared using Sn flux [12]. Theoretical band-structure calculations performed by Cai et al. lead the authors to conclude that the magnetic and electrical properties of $CeCoSb_3$ would be nearly identical to β-$CeNiSb_3$ [9,12]. However, the magnetic, transport, and thermodynamic properties of $CeCoSb_3$ remain uncharacterized. To further extent the study of Ce–transition metal–Sb phases and having the desire to target the interesting physical properties mentioned above, we have grown this phase employing a synthetic procedure similar to that previously described and this will be further elaborated in Section 2 [12]. In this manuscript we present the synthesis, structural characterization, and physical properties for $CeCo(Sn, Sb)_3$.

2. Materials and methods

2.1. Synthesis

Single crystals of $CeCo(Sb, Sn)_3$ were synthesized via the flux-growth method from excess Sn as previously reported [12]. This phase was prepared by placing Ce (99.9%), along with Co powder (99.998%), Sb shot (99.9999%), and Sn shot (99.99+%) into a 2-mL alumina crucible in a 5:5:15 mmolar ratio of Ce:Co:Sb with 3 g of Sn. The crucible was sealed into an evacuated fused-silica tube and was heated to 913 K for 1 day and then heated to 1323 K at a rate of 100 K/h for 3 days. After dwelling at 1323 K for 3 days, the ampoules were cooled to room temperature at a rate of 5.3 K/h. The excess Sn flux was etched using dilute hydrochloric acid and thin, shiny, black

* Corresponding author. Tel.: +1 225 578 269; fax: +1 225 578 3458.
E-mail addresses: jchan@lsu.edu, jalcom@lsu.edu (J.Y. Chan).

0925-8388/$ – see front matter © 2012 Elsevier B.V. All rights reserved.
doi:10.1016/j.jallcom.2012.01.152

Table 1
Crystallographic parameters for $CeCo(Sb, Sn)_3$.

Formula	$CeCo(Sb, Sn)_3$
a (Å)	12.8400(5)
b (Å)	6.1340(5)
c (Å)	12.1060(15)
V (Å^3)	953.48(15)
Z	8
Crystal system	Orthorhombic
Space group	*Pbcm*
θ range (°)	2.6–33.1
μ (mm^{-1})	29.34
Data collection	
Crystal size	0.10 mm × 0.13 mm × 0.22 mm
Measured reflections	11,660
Independent reflections	1779
Reflections with $I > 2\sigma(I)$	1728
R_{int}	0.037
h	−19 to 19
k	−8 to 8
l	−18 to 17
Refinement	
$R_1[F^2 > 2\sigma(F^2)]$[a]	0.048
$wR_2(F^2)$[b]	0.148
Parameters	53
GOOF	1.22
$\Delta\rho_{max}$ (e Å^{-3})	4.94
$\Delta\rho_{min}$ (e Å^{-3})	−3.96

[a] $R_1 = \sum||F_o| - ||F_c||/\sum||F_o||$.

[b] $wR_2 = \left[\sum[w(F_o^2 - F_c^2)]/\sum[w(F_o^2)^2]\right]^{1/2}$.

plate-like crystals were mechanically extracted. The average crystal dimensions for the length, width, and height correspond to ~0.5 mm, ~1 mm, and 3 mm, respectively. The surfaces of all the crystals were observed to be clean with little evidence of flux contamination. No signs of surface oxidation were observed when the crystals were exposed to air and moisture over a period of months.

2.2. Single-crystal X-ray diffraction

Plate-shaped single crystals of $CeCo(Sb, Sn)_3$ were mounted onto glass fiber tip of a goniometer with epoxy and placed on a Nonius Kappa CCD X-ray diffractometer (Mo Kα radiation, λ = 0.71073 Å). A data collection was performed at room temperature and the crystallographic parameters for $CeCo(Sb, Sn)_3$ are listed in Table 1. The orthorhombic Laue symmetry *mmm* and the systematic absences observed led to the initial space group selection of *Pbma*, which transformed to the standard setting of *Pbcm* (No. 57). Direct methods were used to generate the initial structural model using SIR97 and further refinement was conducted using SHELX97 [13,14]. After the refinement of all the atomic positions, the collected data were corrected for absorption and the displacement parameters were refined as anisotropic. Weighting schemes and extinction corrections were applied during the final stages of refinement. The atomic coordinates and anisotropic displacements are provided in Table 2. Selected interatomic distances and angles for $CeCo(Sb, Sn)_3$ are provided in Table 3. It should be noted that attempts to refine the occupancies of both Sn and Sb for a given Wyckoff site simultaneously were unsuccessful, as the X-ray scattering amplitudes for Sn and Sb are very similar. Therefore all positions were refined as pure Sb.

2.3. Elemental analysis

Since X-ray diffraction cannot reliably resolve Sb from Sn, the chemical composition of a clean single crystal of $CeCo(Sb, Sn)_3$ was determined by energy dispersive spectroscopy (EDS) using a Hitachi S-3600N scanning electron microscope (SEM). A total of seven scans were performed using an accelerating voltage of 15 keV with a beam to sample distance of 20 mm. The composition obtained by normalizing all elements to the Ce composition was found to be $CeCo_{0.95(3)}Sn_{0.57(5)}Sb_{2.6(1)}$. The incorporation of Sn for Sb was observed in the structures of $LnNi(Sn, Sb)_3$ (Ln = Pr, Nd, Sm, Gd, and Tb), which were synthesized using a similar strategy as described above [15].

Table 2
Atomic positions and anisotropic displacement parameters for $CeCo(Sb, Sn)_3$ where X = Sb and Sn.

Atom	x	y	z	U_{eq} (Å^2)[a]
Ce1	0.70043(5)	1/4	0	0.01009(19)
Ce2	0.30495(5)	0.26645(10)	3/4	0.00990(18)
Co1	0.10242(8)	0.03361(17)	0.86220(8)	0.0110(2)
X1	0.97323(6)	1/4	0	0.0119(2)
X2	0.78703(6)	0.25615(10)	3/4	0.0107(2)
X3	0.50181(3)	0.50911(8)	0.87653(5)	0.01127(19)
X4	0.21706(6)	1/4	0	0.0107(2)
X5	0.94442(5)	0.88482(11)	3/4	0.0117(2)

[a] U_{eq} is defined as 1/3 of the trace of the orthogonalized U_{ij} tensor.

Table 3
Selected interatomic distances and angles for $CeCo(Sb, Sn)_3$ where X = Sb and Sn.

Interatomic distances (Å)	
Ce1–X1	3.5027(9)
Ce1–X2 (x 2)	3.2245(5)
Ce1–X3 (x 2)	3.3408(7)
Ce1–X3 (x 2)	3.3563(6)
Ce1–X4 (x 2)	3.2448(4)
Ce2–X2	3.2277(9)
Ce2–X2	3.3456(9)
Ce2–X3 (x 2)	3.3092(7)
Ce2–X3 (x 2)	3.3158(7)
Ce2–X4 (x 2)	3.2316(5)
Ce2–X5	3.2832(9)
X3–X3	2.9920(10)
X3–X3	3.0635(10)
X3–X3	3.0674(3)
Co–X1	2.5986(11)
Co–X1	2.7011(11)
Co–X2	2.5993(11)
Co–X4	2.5906(11)
Co–X5	2.6064(11)
Co–X5	2.6168(12)
Co–Co	2.717(2)
Angles (°)	
X3–X3–X3	87.847(19)
X3–X3–X3	90
X3–X3–X3	90
X3–X3–X3	92.126(19)
X5–Co–X1	79.00(3)
X5–Co–X5	80.73(3)
X5–Co–X2	85.61(4)
X5–Co–X4	92.47(7)
X1–Co–X2	95.81(4)
X1–Co–X4	98.16(4)
X2–Co–X4	111.20(4)
X2–Co–X5	113.16(4)
X1–Co–X5	142.98(4)
X5–Co–X4	163.18(5)

2.4. Physical properties

Magnetic data for $CeCo(Sb, Sn)_3$ were collected using a Quantum Design Magnetic Property Measurement System (MPMS). The temperature-dependent magnetic susceptibility data were measured under zero field cooled (ZFC) conditions between 2.25 K and 300 K under an applied magnetic field of 100 Oe. Field dependent magnetization data were measured between 5 K and 200 K with magnetic fields up to 5 T. The electrical resistivity and specific heat capacity data were collected using a Quantum Design Physical Property Measurement System (PPMS). The magnetic fields and the electrical currents were both applied parallel to the height (long direction) of these thin plates.

3. Results and discussion

3.1. Structure

$CeCo(Sb, Sn)_3$ adopts the $LaPdSb_3$ structure-type with lattice parameters $a \sim 12$ Å, $b \sim 6$ Å, and $c \sim 12$ Å [16]. Detailed descriptions of compounds adopting the $LaPdSb_3$ have been provided elsewhere [9,12,15–17]. Therefore, only a brief structural description of $CeCo(Sb, Sn)_3$ is provided below. The $LaPdSb_3$ structure-type is similar to the $CeCrSb_3$ and α-$CeNiSb_3$ structure types [8,18]. As shown in Fig. 1, $CeCo(Sb, Sn)_3$ can be viewed as being built up by inserting Ce atoms between a layer of Co-centered octahedra, $^2_\infty[CoX_2]$ where X = Sb and Sn, and a distorted square net composed of X atoms, $^2_\infty[X]$. A host of X–X interactions within the $^2_\infty[CoX_2]$ layers have been omitted for clarity.

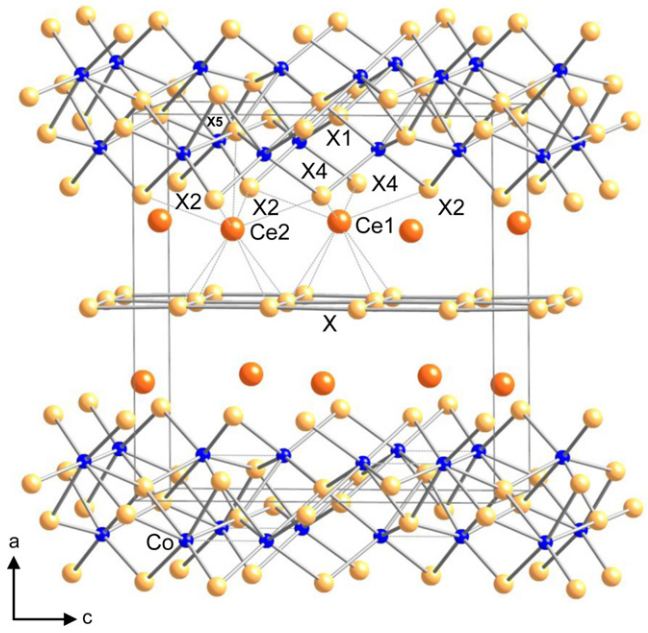

Fig. 1. Crystal structure of $CeCo(Sb, Sb)_3$ where X = Sb and Sn.

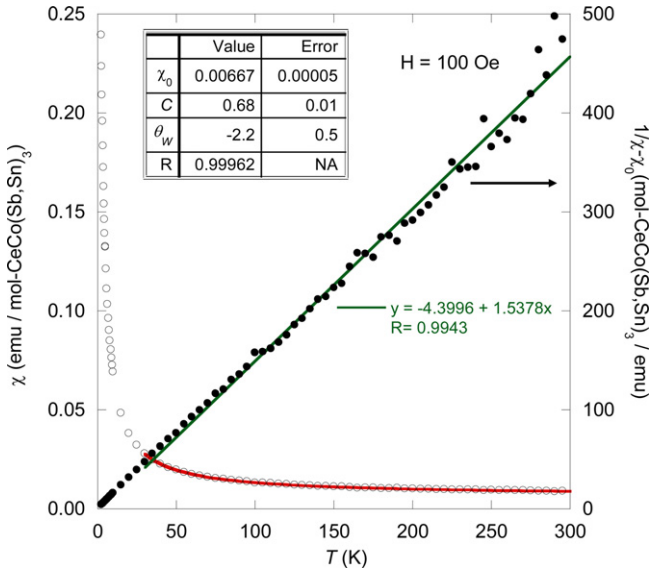

Fig. 2. Temperature dependent magnetic susceptibility, $\chi = M/H$, of $CeCo(Sb, Sn)_3$ under an applied field of 100 Oe is shown on the left axis, and the inverse magnetic susceptibility, $1/\chi - \chi_0$, as a function of temperature is shown on the right axis. The χ_0, C, and θ_W parameters which were obtained from a modified Curie–Weiss fit to the magnetic susceptibility can be viewed in the inset table of this figure.

$CeCo(Sb, Sn)_3$ contains two crystallographically inequivalent Ce sites with slightly different coordination environments. The Ce1 atoms are surrounded by 8 X atoms, adopting a square antiprismatic geometry, where 4 atoms of the $^2_\infty[X]$ layer form a square base, and 4 X atoms from the $^2_\infty[CoX_2]$ layer form a square directly above, but twisted 45° with respect to the square of the $^2_\infty[X]$ layer. The Ce2 atoms are surrounded by 9 X atoms and adopt a monocapped square antiprismatic geometry with an additional X5 atom capping the second square formed by the $^2_\infty[XSb_2]$ layer. The X1 atom in the capping position of Ce1 is considered too far from the Ce1 atom for any considerable bonding interactions. The main structural distinction between $CeCrSb_3$, α-$CeNiSb_3$, and $CeCo(Sb, Sn)_3$ lies in the packing of the $^2_\infty[TSb_2]$ octahedral layer along the [0 0 1] direction [8,18]. The $^2_\infty[CoX_2]$ octahedra in $CeCo(Sb, Sn)_3$ are edge-sharing in [0 1 0], whereas they are face-sharing, with every other octahedron sharing edges in [0 0 1]. The angles between the Co and X atoms diverge considerably from the ideal 90°. Furthermore, Co–Co interactions are present at the adjourning octahedral faces with a distance of 2.717(2) Å.

3.2. Physical properties

The temperature-dependent magnetic susceptibility of $CeCo(Sb, Sn)_3$ in a field of 100 Oe is shown in Fig. 2. The modified Curie–Weiss form, $\chi(T) = \chi_0 + C/(T - \theta_W)$, where C is the Curie constant, θ_W represents the Weiss temperature, and χ_0 accounts for the temperature independent contributions to the magnetic susceptibility due to Pauli paramagnetism and Larmor diamagnetism, was used to fit the magnetic susceptibility data for 30–300 K. The values and errors for the parameters obtained from the fit of the modified Curie–Weiss form to the data are displayed in the inset table of Fig. 2. The value of χ_0 thus obtained was subtracted from χ, and the inverse of $\chi - \chi_0$ is plotted on the right axis of Fig. 2. A linear fit to these data from 30 K to 300 K was performed to attempt to extract more accurate values for C and θ_W. The effective moment obtained from C, 2.28 μ_B/mol-Ce, was compared to the calculated value using $\mu_{eff} = g_J[J(J+1)]^{1/2}\ \mu_B$ or 2.54 μ_B/mol-Ce for a free Ce^{3+} ion. Similar to what was observed for isostructural β-$CeNiSb_3$ the effective moment in $CeCo(Sb, Sn)_3$ is somewhat smaller than the expected value for a Ce^{3+} ion indicating that there is likely no magnetic moment associated with the transition metal site (Co) [9]. In addition, a small negative Weiss temperature of −2.2 K was obtained from fits to the magnetic susceptibility using the modified Curie–Weiss equation, while a small positive Weiss temperature of 2.9 K was obtained from linear fits to the inverse $\chi - \chi_0$ data. These data indicate a small Weiss temperature, however, the variation in the values obtained indicate that there may be systematic error of order a few Kelvin in our method for determining θ_W.

The magnetic properties of this system were further probed by measuring the field-dependent magnetization for fields of up to 5 T at temperatures between 5 and 200 K (Fig. 3a). The magnetization data above 5 K is linear and shows no sign of saturation, whereas the data at 5 K show a tendency towards saturation at high fields as expected for a paramagnet. Fig. 3b–d display the field-dependent magnetization curves vs. $H/T - \theta$ for $\theta = 0$ K, +2 K, and −2 K to explore the sign and magnitude of the magnetic exchange interaction between Ce magnetic moments. As can be seen in Fig. 3b, the data scale best when plotted against H/T suggestive of weak correlations on the order of magnitude of 1 K. The quality of the scaling is visibly reduced when we include a small ferromagnetic coupling, as shown in Fig. 3d, so that we conclude that our magnetization data does not support ferromagnetic correlations between the magnetic ions.

The electrical resistivity as a function of temperature for $CeCo(Sb, Sn)_3$ is displayed in Fig. 4. The resistivity is nearly temperature independent below room temperature with a value above 200 μΩ cm indicating disordered metallic transport as would perhaps be expected for a material with partial Sn occupation of the X site. Below 10 K a decreasing ρ with T is observed. Because we suspect Kondo lattice behavior for this Ce compound, we plot ρ as a function of $\ln T$ in the inset of Fig. 4 where linearity is apparent, although the T-range is limited. Our identification of the upturn in the resistivity at low temperatures as a Kondo feature is further supported by the negative magnetoresistance, $\rho(H) - \rho(H=0)/\rho(H=0)$, that we observe at $T = 1.5$ K and $T = 6$ K as shown in Fig. 5. A negative magnetoresistance that increases in magnitude with decreasing temperature is expected in the incoherent magnetic scattering regime [19]. Additionally, the inset of Fig. 5 shows that the isothermal curves scale

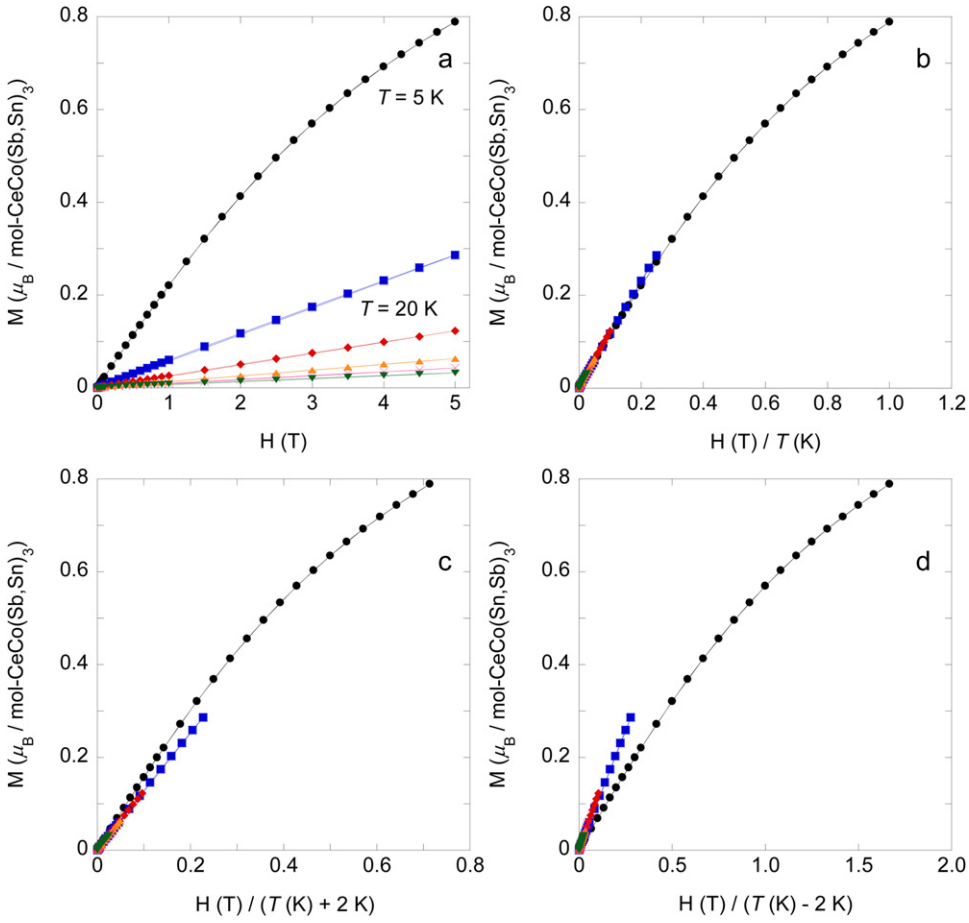

Fig. 3. (a) Magnetization (M) of CeCo(Sb, Sn)$_3$ as a function of applied field (H) at 5 K, 20 K, 50 K, 100 K, 150 K, and 200 K. (b) Magnetization vs. field divided by temperature (H/T). (c) Magnetization vs. $H/T+2$ K. (d) Magnetization vs. $H/T-2$ K. The circles, squares, diamonds, triangles, crosses, and upside down triangles represent the magnetic isotherms at $T=5$ K, 20 K, 50 K, 100 K, 150 K, and 200 K, respectively.

well when the magnetic field values are normalized by $(T+T^*)$ where $T^*=2$ K. The overlap between the two isothermal magnetoresistance curves shown in the inset of Fig. 5 by a 2 K scaling factor is suggestive of a low Kondo temperature for CeCo(Sb, Sn)$_3$.

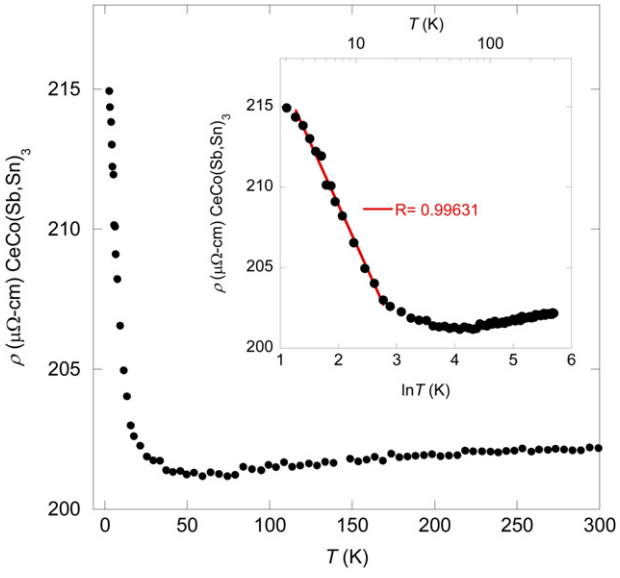

Fig. 4. Temperature-dependent electrical resistivity (ρ) for CeCo(Sb, Sn)$_3$. The inset shows a linear fit of ρ vs. ln T for CeCo(Sb, Sn)$_3$ from 3 K to 10 K.

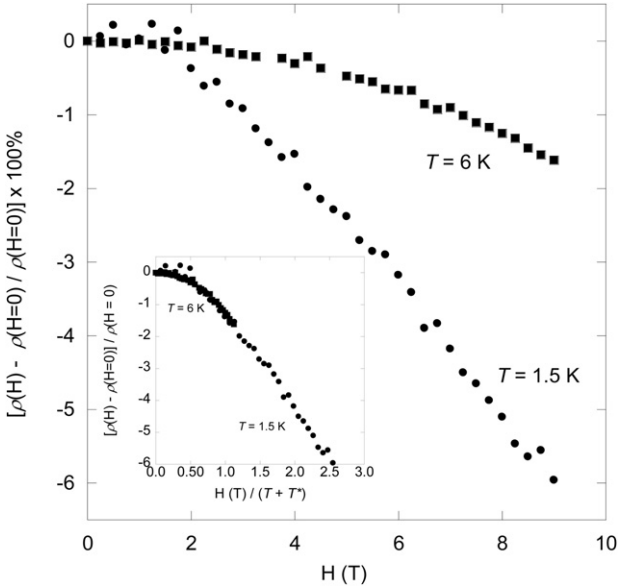

Fig. 5. Magnetoresistance, $[\rho(H)-\rho(H=0)/\rho(H=0)]\times 100\%$, as a function of applied field at $T=1.5$ K (circles) and $T=6$ K (squares). The inset shows magnetoresistances at $T=1.5$ K (circles) and $T=6$ K (squares) as a function of $H(T)/(T-T^*)$.

Perhaps more informative is the specific heat capacity (C_p) displayed as a function of temperature for CeCo(Sb, Sn)$_3$ in Fig. 6. We observe a phase transition at $T\sim 2$ K which is more apparent in the inset of Fig. 6 where the low temperature data is presented

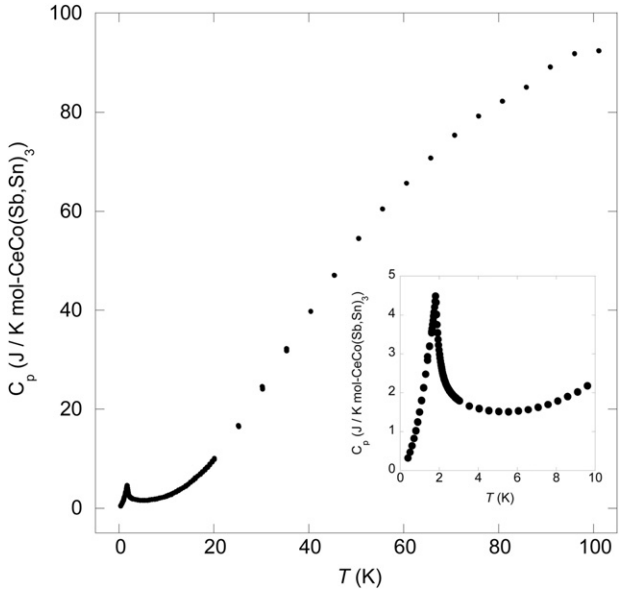

Fig. 6. Specific heat capacity (C_p) for CeCo(Sb, Sn)$_3$ as a function of temperature. The inset serves to highlight the thermodynamic phase transition.

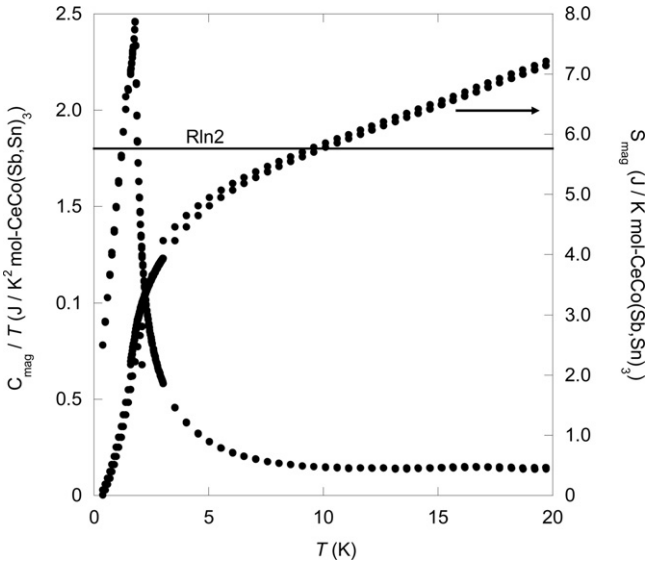

Fig. 8. Magnetic heat capacity divided by temperature (C_{mag}/T) and magnetic entropy (S_{mag}) as a function of temperature. Rln2 is indicated by the line.

on a finer scale. This sharp peak found at a low temperature is likely a magnetic phase transition which is not inconsistent with the small θ_W values obtained from the susceptibility and our scaling of the magnetization data (Fig. 3). Fits of the standard metallic form, $C_p/T = \gamma + \beta T^2$, to our C_p/T vs. T^2 data from 100 K^2 to 400 K^2 for CeCo(Sb, Sn)$_3$ were performed to extract the β and γ coefficients as shown in Fig. 7. The best fit values for β and γ obtained from this procedure were 0.85 mJ/mol-K^4 and 140 mJ/mol-K^2, respectively. The value of γ indicated by our fitting procedure is considerable larger than that found in simple metals such as Cu ($\gamma \sim 1$ mJ/mol-K^2), and would imply the formation of a heavy Fermion metallic state [20–23]. To further assess this possibility we estimated the magnetic heat capacity (C_{mag}) by subtracting βT^3 from the specific heat capacity (C_p). The magnetic heat capacity divided by temperature (C_{mag}/T) and the magnetic entropy (S_{mag}) determined by integrating C_{mag}/T are shown on the left and right axes of Fig. 8, respectively. Here, we observe that the entropy increases sharply from our lowest temperatures up to 5 K while it continues to increase with T at a smaller rate above 5 K. The entropy expected for a $S = 1/2$, magnetic moment is exceeded above 10 K confirming that the phase transition observed at 2 K is likely magnetic in origin.

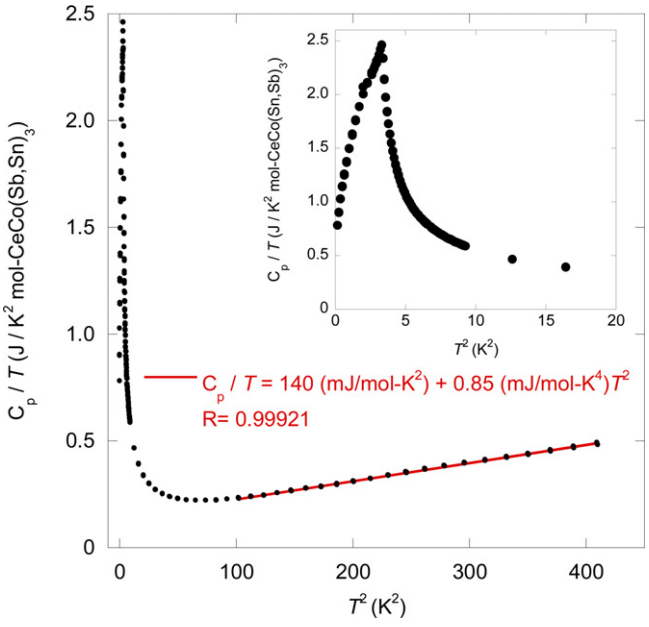

Fig. 7. A plot of C_p/T vs. T^2 for CeCo(Sb, Sn)$_3$. The inset serves to highlight the thermodynamic phase transition.

4. Conclusion

Single crystals of CeCo(Sb, Sn)$_3$ where grown via the flux-growth method using excess Sn. These crystals were characterized by single crystal X-ray diffraction and a more accurate composition of these crystals was determined by EDS. We have shown that the magnetic susceptibility of CeCo(Sb, Sn)$_3$ is paramagnetic down to the lowest temperature measured. The Curie–Weiss analysis and magnetization scaling suggest weak magnetic correlations become relevant on the order of magnitude 1 K. This is further supported by our analysis of the heat capacity data which indicate a magnetic transition near 2 K. Additionally, the low temperature resistivity and MR% behavior of CeCo(Sb, Sn)$_3$ are consistent with incoherent Kondo scattering of the conducting electrons [19]. A standard analysis of the heat capacity data indicates that CeCo(Sb, Sn)$_3$ has enhanced charge carries mass, $\gamma = 140$ mJ/mol-K^2. However, this is inconsistent with a low Kondo temperature and the absence of a coherence observed in the resistivity. Furthermore, the negative magnetoresistance values at low temperatures for CeCo(Sb, Sn)$_3$ are also not consistent with a coherent heavy Fermion metallic state where a positive magnetoresistance has been observed in a number heavy-fermion compounds [19,24]. Gschneidner et al. [25] have proposed that large, nearly linear, contributions to the specific heat occur as a result of low lying crystal field levels. In this case a large γ is confused with the tail of a higher temperature Schottky peak which results from the crystal field splitting of the Ce f-levels. Low lying crystal field levels have been observed in $CeCd_{11}$ (3 doublets – 0 K, 17.5 K, and 80 K) and $CeGa_2$ (3 doublets – 0 K, 62.5 K and 310 K) which give rise to erroneously large Sommerfeld coefficients (γ) [25–27]. That our magnetic entropy for CeCo(Sb, Sn)$_3$ displays a continuously increase beyond Rln2 may be indicative of contributions from low lying crystal field levels similar to what has been observed in $CeMg_3$ [28]. In view of both our resistivity and magnetoresistance data which indicate an absence of a coherent heavy Fermion state, we conclude that the enhanced Sommerfeld

coefficient, $\gamma = 140$ mJ/mol-K^2, indicated from the standard analysis of the specific heat data for CeCo(Sb, Sn)$_3$ is likely a result of low lying crystal field levels rather than the formation of heavy quasiparticles.

Acknowledgements

JFD and JYC would like to acknowledge support for this research from the National Science Foundation (NSF) through DMR0804376 and DMR1063735, respectively.

Appendix A. Supplementary data

Supplementary data associated with this article can be found, in the online version, at doi:10.1016/j.jallcom.2012.01.152.

References

[1] H. Kleinke, Chem. Soc. Rev. 29 (2000) 411–418.
[2] A.M. Mills, R. Lam, M.J. Ferguson, L. Deakin, A. Mar, Coordin. Chem. Rev. 233–234 (2002) 207–222.
[3] G.A. Papoian, R. Hoffmann, Angew. Chem. Int. Ed. 39 (2000) 2409–2448.
[4] E.L. Thomas, J.N. Millican, E.K. Okudzeto, J.Y. Chan, Comments Inorg. Chem. 27 (2006) 1–39.
[5] S.M. Kauzlarich, S.R. Brown, G.J. Snyder, Dalton Trans. 209 (2007) 2099–2107.
[6] W.A. Phelan, M.C. Menard, M.J. Kangas, G.T. McCandless, B.L. Drake, J.Y. Chan, Chem. Mater 24 (2012) 409–420.
[7] A.S. Sefat, S.L. Bud'ko, P.C. Canfield, J. Magn. Magn. Mater. 320 (2008) 120–141.
[8] R.T. Macaluso, D.M. Wells, R.E. Sykora, T.E. Albrecht-Schmitt, A. Mar, S. Nakatsuji, H. Lee, Z. Fisk, J.Y.J. Chan, Solid State Chem. 177 (2004) 293–298.
[9] E.L. Thomas, D.P. Gautreaux, H.O. Lee, Z. Fisk, J.Y. Chan, Inorg. Chem. 46 (2007) 3010–3016.
[10] N.B. Perkins, J.R. Iglesias, M.D. Nunez-Regueiro, B. Coqblin, EPL-Europhys. Lett. 79 (2007) 57006.
[11] V.A. Sidorov, E.D. Bauer, H. Lee, S. Nakatsuji, J.D. Thompson, Z. Fisk, Phys. Rev. B. 71 (2005) 094422.
[12] W.-Z. Cai, L.-M. Wu, L.-H. Li, L. Chen, Eur. J. Inorg. Chem. 2009 (2009) 230–237.
[13] A. Altomare, M.C. Burla, M. Camalli, G.L. Cascarano, C. Giacovazzo, A. Guagliardi, A.G.G. Moliterni, G. Polidori, R. Spagna, J. Appl. Crystallogr. 32 (1999) 115–119.
[14] G.M. Sheldrick, Acta Crystallogr. A 64 (2008) 112–122.
[15] D.P. Gautreaux, C. Capan, J.F. DiTusa, D.P. Young, J.Y.J. Chan, Solid State Chem. 181 (2008) 1977–1982.
[16] E.L. Thomas, D.P. Gautreaux, J.Y. Chan, Acta Crystallogr. Sect. E: Struct. Rep. E 62 (2006) I96–I98.
[17] W.A. Phelan, G.V. Nguyen, A.B. Karki, D.P. Young, J.Y. Chan, Dalton Trans. 39 (2010) 6403–6409.
[18] M. Brylak, W. Jeitschko, Naturforsch. B. 50 (1995) 899–904.
[19] U. Rauchschwalbe, F. Steglich, H. Rietschel, Physica B. & C 148 (1987) 33–36.
[20] Z. Fisk, D.W. Hess, C.J. Pethick, D. Pines, J.L. Smith, J.D. Thompson, J.O. Willis, Science 239 (1988) 33–42.
[21] Z. Fisk, H.R. Ott, T.M. Rice, J.L. Smith, Nature 320 (1986) 124–129.
[22] Z. Fisk, J.L. Sarrao, J.L. Smith, J.D. Thompson, Proc. Natl. Acad. Sci. U.S.A. 92 (1995) 6663–6667.
[23] Z. Fisk, J.L. Sarrao, J.D. Thompson, Curr Opin Solid State Mater. Sci. 1 (1996) 42–46.
[24] G. Oomi, T. Kagayama, Physica B 201 (1994) 235–238.
[25] K.A. Gschneidner, J. Tang, S.K. Dhar, A. Goldman, Physica B 163 (1990) 507–510.
[26] J. Tang, K.A. Gschneidner, J. Magn. Magn. Mater. 75 (1988) 355–360.
[27] P. Burlet, M.A. Fremy, D. Gignoux, G. Lapertot, S. Quezel, L.P. Regnault, J. Rossatmignod, E. Roudaut, J. Magn. Magn. Mater. 63–4 (1987) 34–36.
[28] P.K. Das, N. Kumar, R. Kulkarni, A. Thamizhavel, Phys. Rev. B. 83 (2011) 134416.